Bearing Damage Detection via Wavelet Packet Decomposition of the Stator Current

Levent Eren, *Member, IEEE,* and Michael J. Devaney, *Member, IEEE*

***Abstract*—Bearing faults are one of the major causes of motor failures. The bearing defects induce vibration, resulting in the modulation of the stator current. In this paper, the stator current is analyzed via wavelet packet decomposition to detect bearing defects. The proposed method enables the analysis of frequency bands that can accommodate the rotational speed dependence of the bearing defect frequencies. The wavelet packet decomposition also provides a better treatment of nonstationary stator current than currently used Fourier techniques.**

***Index Terms*—Bearing fault detection, condition monitoring, induction motors, motor current signature analysis (MCSA).**

I. Introduction

INDUCTION machines are used widely in industrial manufacturing plants. The industry's heavy reliance on these machines in critical applications makes catastrophic motor failures very expensive. Therefore, a significant amount of research effort is focused on the preventive maintenance of motors. Motor current signature analysis (MCSA) provides a nonintrusive way to assess the health of a machine. The steady-state current of an induction motor is analyzed via the discrete wavelet packet transform to detect faulty bearings in this study.

The bearing-related information is obtained by determining the current spectral frequencies induced by the characteristic vibration frequencies. The relationship of bearing vibration to stator current spectrum results from the fact that any air gap eccentricity produces anomalies in the air gap flux density [1]. The characteristic vibration frequencies due to bearing defects can be calculated from the rotor speed and the bearing geometry. The typical rolling element bearing geometry is displayed in Fig. 1. The characteristic vibration frequencies, f_v can be calculated using (1)–(4) [2].

The outer race defect frequency, $f_{\rm OD}$, the ball passing frequency on the outer race, is given by

$$f_{\rm OD} = \frac{n}{2} f_{\rm rm} \left(1 - \frac{\rm BD}{\rm PD} \cos\phi\right) \tag{1}$$

where φ is the contact angle, PD is the pitch diameter, BD is the ball diameter, n is the number of balls, and $f_{\rm rm}$ is the rotational speed.

Manuscript received June 15, 2002; revised November 16, 2003.

L. Eren is with the Department of Electrical and Electronics Engineering, University of Bahcesehir, Bahcesehir, Istanbul 34538, Turkey (e-mail: leren@bahcesehir.edu.tr).

M. J. Devaney is with the Department of Electrical and Computer Engineering, University of Missouri, Columbia, MO 65211 USA (e-mail: DevaneyM@missouri.edu).

Digital Object Identifier 10.1109/TIM.2004.823323

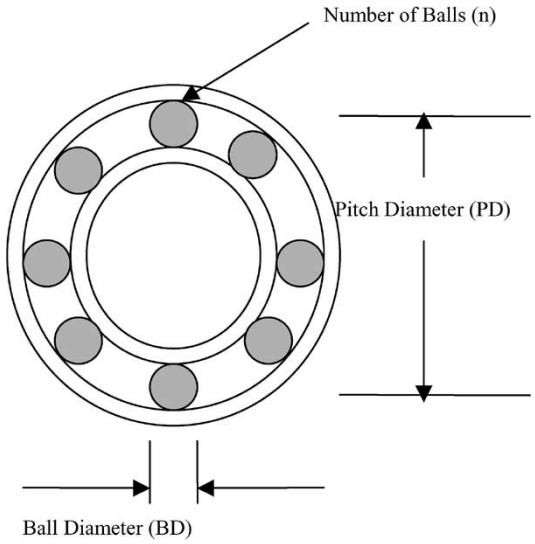

Fig. 1. Rolling element bearing geometry.

The inner race defect frequency, $f_{\rm ID}$, the ball passing frequency on the inner race, is given by

$$f_{\rm ID} = \frac{n}{2} f_{\rm rm} \left(1 + \frac{\rm BD}{\rm PD} \cos\phi\right). \tag{2}$$

The ball defect frequency, $f_{\rm BD}$, the ball spin frequency, is given by

$$f_{\rm BD} = \frac{\rm PD}{2\rm BD} f_{\rm rm} \left(1 - \left(\frac{\rm BD}{\rm PD}\right)^2 \cos^2\phi\right). \tag{3}$$

The train defect frequency, $f_{\rm TD}$, caused by an irregularity in the train, is given by

$$f_{\rm TD} = \frac{1}{2} f_{\rm rm} \left(1 - \frac{\rm BD}{\rm PD} \cos\phi\right). \tag{4}$$

The characteristic current frequencies, f_{CF}, due to the bearing characteristic vibration frequencies, f_v, are calculated by [1]

$$f_{CF} = |f_e \pm m f_v| \tag{5}$$

where $m = 1, 2, 3, \ldots$ and f_e is the power line frequency. This latter equation represents an amplitude modulation of the stator current by the bearing vibrations.

Equations (1)–(5) can be used to calculate the current spectral components due to faulty bearings. In traditional MCSA, the Fourier transform is utilized to determine the current spectrum. Then, the bearing defect induced frequencies are identified and

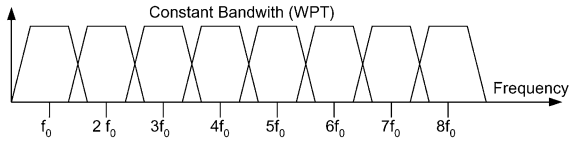

Fig. 2. Linear frequency separation.

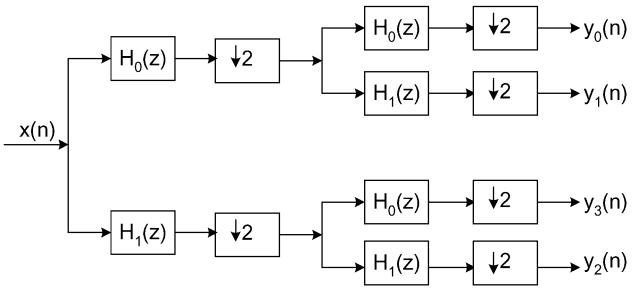

Fig. 3. Analysis part of wavelet packet filter bank.

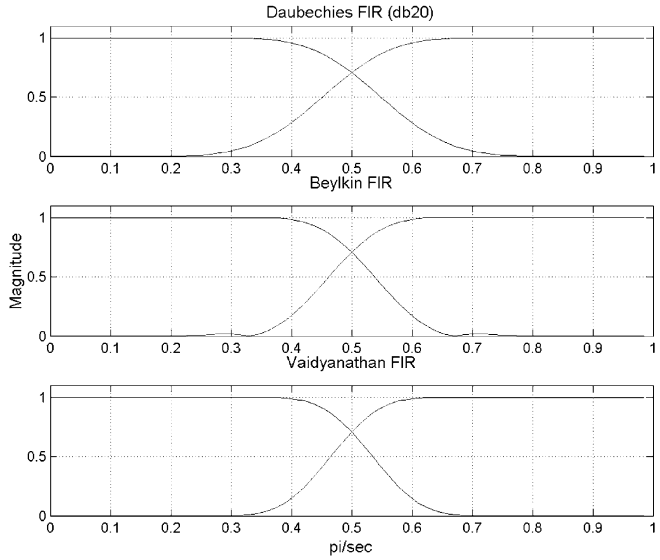

Fig. 4. Frequency roll-off characteristics of various FIR filters.

compared with initial measurements to detect any deterioration in bearing health. The shortcoming of this approach is that the Fourier analysis is limited to stationary signals and the stator current is nonstationary by nature.

In this study, the wavelet packet decomposition of the motor current signal is proposed as an alternate approach. The wavelet packet transform provides better analysis for nonstationary signals and permits tailoring of the frequency bands to cover the range of bearing-defect induced frequencies resulting from rotor speed variations. In this approach, the rms values for defect frequency bands are compared with baseline readings to determine any degradation in bearing health.

The discrete wavelet transform has been successfully applied to the analysis of both transient and steady-state power system signals [3], [4]. Recently, the wavelet packet decomposition was also utilized to detect induction motor mechanical faults such as broken rotor bars and air gap eccentricity from its current signature [5].

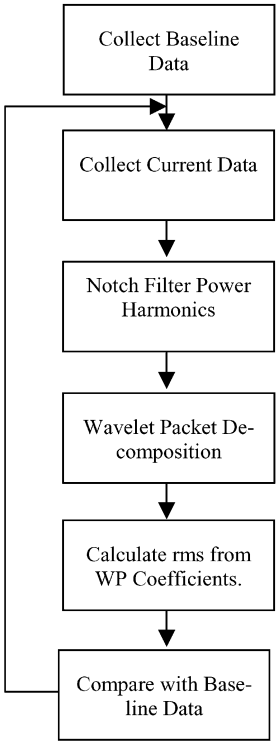

Fig. 5. Analysis process algorithm.

Fig. 6. Outer race defect.

II. Proposed Method

Today, the wavelet theory represents a collection of work done largely independently in various fields such as mathematics, physics, and engineering. Wavelets, filter banks, and multiresolution signal analysis, which have been used independently in the fields of mathematics, signal processing, and computer vision, respectively, have recently converged to form a single theory [6]. The wavelet transform (WT) provides an alternative to the short-time Fourier transform (STFT) in nonstationary signal processing. In contrast to the fixed analysis window size in the STFT, the WT uses longer windows for low frequencies and shorter windows for higher frequencies. Finer frequency resolution may be achieved via the wavelet

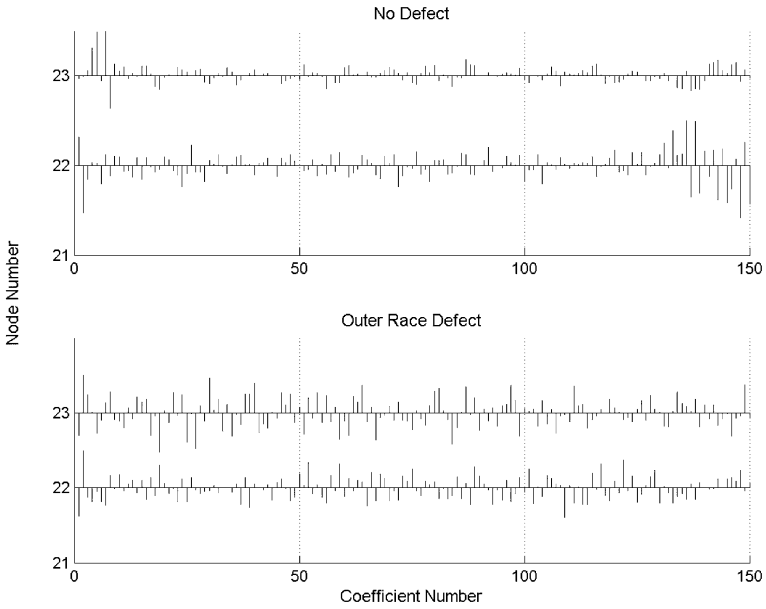

Fig. 7. WPC plots for race defect and no defect.

packet transform (WPT). Wavelet transform and multirate filter banks are closely related. Multirate filter banks give the structures required to generate important cases of wavelets and the wavelet transform [7].

Subband decomposition of signals using two-band filter banks can be implemented efficiently and conveniently [8]. Daubechies also showed that the following equations can be used to numerically obtain wavelet and scaling coefficients

$$\psi_{j,k}(x) = 2^{-j/2}\psi(2^{-j}x - k). \tag{6}$$

The wavelet coefficients for level j can be obtained from scaling coefficients from level $j-1$ using

$$\psi_{j,k}(x) = \sum_n g_{n-2k}\phi_{j-1,n}(x) \tag{7}$$

$$\langle f, \psi_{j,k}\rangle = \sum_n \overline{g_{n-2k}}\,\langle f, \phi_{j-1,n}\rangle\,. \tag{8}$$

The scaling coefficients for level j can be obtained from the scaling coefficients for level $j-1$ using

$$\phi_{j,k}(x) = \sum_n h_{n-2k}\phi_{j-1,n}(x) \tag{9}$$

$$\langle f, \phi_{j,k}\rangle = \sum_n \overline{h_{n-2k}}\,\langle f, \phi_{j-1,n}\rangle\,. \tag{10}$$

Where g and h are high-pass and low-pass filters, respectively. The procedure can start by calculating $\langle f, \psi_{1,k}\rangle$ and $\langle f, \phi_{1,k}\rangle$ from $\langle f, \phi_{0,n}\rangle$ using (8) and (10), respectively. Then, the same procedure is used until the level j is reached.

Wavelet analysis provided improved signal processing for transient signal analysis. It results in better time localization in higher frequencies in return for poorer frequency resolution. Coifman, Meyer, and Wickerhauser introduced wavelet packet analysis to improve the poor frequency resolution at high frequencies [9]. They basically generalized the link between multiresolution and wavelets. Wavelet packet analysis offers a more efficient decomposition for signals containing both transient and stationary components. The frequency separation obtained by wavelet packet decomposition is depicted in Fig. 2. It is very similar to that of the STFT. Here, the wavelet bases W_j are decomposed into approximation spaces W_{j+1}^0 and W_{j+1}^1. The wavelet filter bank structure to accomplish such decomposition is depicted in Fig. 3.

TABLE I
RMS VALUES CALCULATED FOR HEALTHY AND FAULTY BEARINGS FOR OUTER RACE DEFECT

	Healthy		*Faulty*	
	mean	*std*	*mean*	*std*
Node 22	0.0074	0.0025	0.0235	0.0008
Node 23	0.0099	0.0052	0.0119	0.0024

The wavelet packet coefficients $d_{j,k}^p$ can be used to calculate the rms value of any node (j,p)

$$x_{\mathrm{rms}}(j,p) = \sqrt{\sum_k \left(d_{j,k}^p\right)^2} \tag{11}$$

where

$$d_{j+1}^{2p}[k] = d_j^p[k] * \bar{h_0}[2k] \tag{12}$$

and

$$d_{j+1}^{2p+1}[k] = d_j^p[k] * \bar{h_1}[2k] \tag{13}$$

can be used repeatedly to obtain all the wavelet packet coefficients.

The filter selection for the wavelet packet filter-bank is important since it determines the frequency separation and computational complexity of the filter-bank structure. Here, the Vaidyanathan FIR filter [10] was selected after reviewing the performance of various FIR filters. It provides better frequency separation than both Daubechies and Beylkin filters. Although the Beylkin filter requires less computational effort,

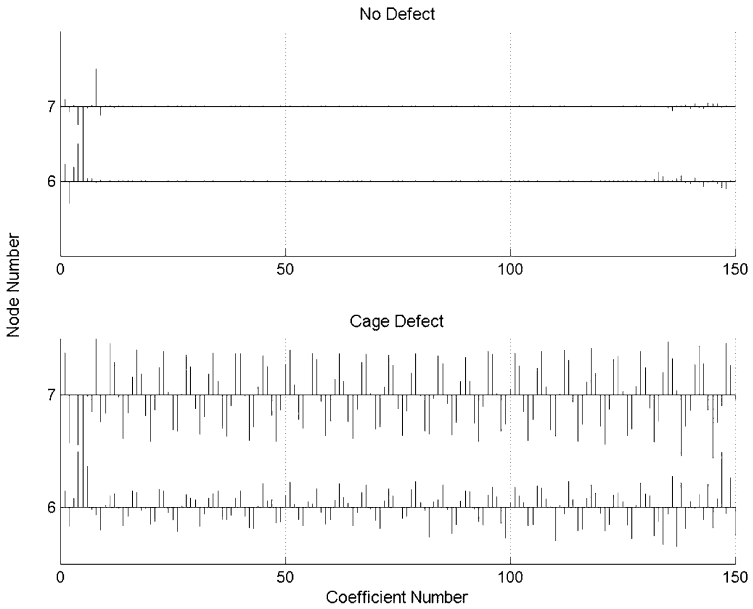

Fig. 8. WPC plots for cage defect and no defect.

the Vaidyanathan filter is selected to minimize the leakage from the adjacent frequency bands. The frequency roll-off characteristics of some popular FIR filters are depicted in Fig. 4.

The wavelet packet decomposition of the motor current signal is the proposed method of signature analysis in this study. For a four-pole machine at 60 Hz, the first harmonics for the vibrations for all the bearing defects listed previously will result in characteristic current frequency components in 0–240 Hz frequency band. Therefore, the current signal can be decomposed linearly within the 0–240 Hz band and decomposed logarithmically for higher frequency bands to minimize the computational effort.

The major steps of the data analysis procedure are shown in Fig. 5. First, the stator current data is sampled at 32 points per cycle for 15 s at 60 Hz. The sampled current signal contains the power system fundamental and third harmonic components. The bearing defect induced current spectrum components are significantly smaller than the power system harmonics in magnitude, therefore, some preprocessing of the signal is required to suppress the power system harmonics before the current signal is analyzed via wavelet packet analysis. The fundamental and third power frequency harmonics are both notch filtered to minimize the error due to their leakage. If the bearing induced frequencies at certain loading level are very close to the power system harmonics, the analysis may be performed at other load levels.

In the next stage, the current signal is decomposed into 7.5-Hz wavelet packets for the 0–240 Hz frequency band using a Vaidyanathan FIR filter-bank structure. After the wavelet packet coefficients are obtained, the node rms values are computed using the wavelet packet coefficients. Due to the computational complexity involved in such decomposition, the algorithm may be implemented in a circuit monitor to perform the analysis at certain time intervals. Bearing health deteriorates over a long period of time; therefore, real-time monitoring is not needed.

The linear decomposition of the signal for 0–240 Hz band can be obtained by the analysis filter-bank depicted in Fig. 3. Here, H_0 and H_1 are the low-pass and high-pass filters, respectively.

TABLE II
RMS VALUES CALCULATED FOR HEALTHY AND FAULTY BEARINGS FOR CAGE DEFECT

	Healthy		*Faulty*	
	mean	*std*	*mean*	*std*
Node 5	0.0396	0.0097	0.1099	0.0030
Node 7	0.0275	0.0084	0.1635	0.0307

It should be noted that $y2$ and $y3$ are reversed in the figure. This is due to the natural, or Paley, order produced by the algorithm. The algorithm may be easily modified to produce a sequence ordered wavelet packet analysis [9]. The linear decomposition obtained from wavelet packet decomposition is depicted in Fig. 2. In this figure, f_0 is the frequency bandwidth required for the analysis. In our case, the frequency range of 0–240 Hz is decomposed into 7.5-Hz bands.

In the proposed approach, the signal rms values for defect frequency bands are recorded for a healthy set of bearings to serve as baseline data. Then, the new readings are compared with previous readings to determine any degradation in the bearing health. Readings that are two standard deviations higher than the baseline readings may be flagged as defective.

III. TESTING AND RESULTS

A three-phase, 1 hp, 200 V, 60 Hz, 1750 rpm, four-pole induction motor was used in this study (US Motors Frame 143T). The shaft end ball bearing is a 6205–2Z-J/C3 (nine balls) and the opposite end ball bearing is a 6203–2Z-J/C3 (seven balls). Two types of bearing faults were studied in the evaluation: outer race defects and cage defects.

In testing, the steady state motor current data were captured, at 32 points per cycle for 15 s, using a Square D series 4000 Circuit Monitor with the machine at no load before and after the fault was introduced. The captured signals were first notch

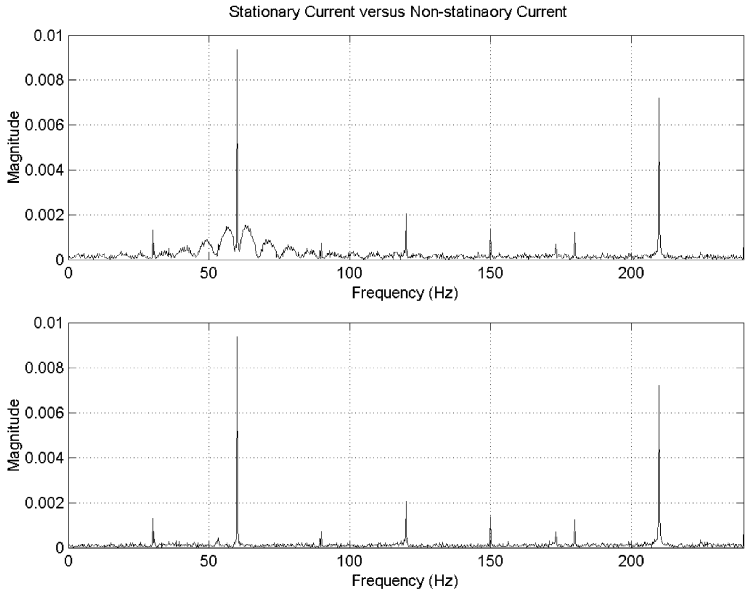

Fig. 9. Fourier spectrums of stationary and nonstationary currents.

filtered to remove power system harmonics. Then, the data were analyzed using the wavelet packet transform. Finally wavelet packet coefficients were used to calculate the rms values.

In the first test, the outer race defect was explored. A one mm diameter hole was drilled on the outer race to simulate an outer race defect. The bearing outer race defect characteristic vibration frequency at no load speed (1798 r/min) is 108 Hz. The corresponding current spectrum components are at 48 and 168 Hz, respectively. The 168-Hz frequency component was selected for analysis since it is further away from the power system fundamental harmonic and rotor speed eccentricity fundamental components ($60 \pm f_{\mathrm{rm}}$). The bearing with the outer race defect is depicted in Fig. 6.

Nodes 22 and 23 were selected for the analysis. These two nodes contain 157.5–165-Hz and 165–172.5-Hz frequency bands, respectively. The wavelet packet coefficients for tests with a healthy and a faulty shaft-end bearing are plotted in Fig. 7.

The wavelet coefficients for nodes 22 and 23 are used to calculate the rms values for the frequency bands of interest. The mean and standard deviation for the specified nodes were calculated from eight healthy bearing trials. The mean values are 0.0074 and 0.0099 for nodes 22 and 23, respectively. The corresponding standard deviation values are 0.0025 and 0.0052. The mean and standard deviation for the specified nodes were calculated from three faulty bearing trials. The mean values are 0.0235 and 0.0119 for nodes 22 and 23, respectively. The corresponding standard deviation values are 0.0008 and 0.0024.

The resulting mean and standard deviation values for both cases are given in Table I. The data indicates an increase in rms values for nodes 22 and 23 for the faulty bearings of 217.7% and 20.9%, respectively. In the second test, the cage defect was explored. The cage was dented to simulate a cage defect. The bearing cage defect characteristic vibration frequency at no load speed (1798 r/min) is 12 Hz. Corresponding current spectrum components are at 48 and 72 Hz, respectively. In this case, either component can be selected since they are equally separated from the power system fundamental harmonic. The 48-Hz component was selected for the analysis. As a result, nodes 5 and 7 were selected. These two nodes contain the 37.5–45-Hz and 45–52.5-Hz frequency bands, respectively. The wavelet packet coefficients for tests with a healthy and a faulty shaft-end bearing are plotted in Fig. 8.

The wavelet coefficients for nodes 5 and 7 are used to calculate the rms values for the specified frequency bands. The mean and standard deviation for the specified nodes were calculated using eight trials for the healthy baseline data. The mean values are 0.0396 and 0.0275 for nodes 5 and 7, respectively. The corresponding standard deviation values are 0.0097 and 0.0084. The mean and standard deviation for the specified nodes were also calculated from eight faulty bearing trials. The mean values are 0.1099 and 0.1635 for nodes 5 and 7, respectively. The corresponding standard deviation values are 0.0030 and 0.0307.

The resulting mean and standard deviation values for both cases are given in Table II. The data indicates that rms values for both nodes 5 and 7 are elevated for the faulty bearings by 177.6% and 494.5%, respectively.

When pre-fault and post-fault bearing current signals are compared under the steady state conditions, significant energy increase is detected in node 22 and node 7 for outer race and cage defects, respectively. In both cases, the results are more than two standard deviations higher than the baseline data indicating the fault conditions.

In a final test, stationary and nonstationary current waveforms for a healthy bearing set are also analyzed by both FFT and wavelet packet decomposition techniques. The results of the FFT analysis are depicted in Fig. 9. The upper plot displays the spectrum of the nonstationary waveform, whereas the lower plot displays the spectrum of the stationary waveform. It is obvious from the figure that the nonstationary waveform caused by speed variations may result in a healthy bearing to be flagged as faulty (cage fault). In the case of the wavelet packet decomposition, the rms levels do not increase as much; therefore, there is a smaller possibility of misdetection.

IV. Conclusion

Multifunction circuit monitors are finding increased use in monitoring individual motor loads. The current data that they provide can be regularly evaluated for a useful predictive maintenance bearing diagnostic when analyzed by the discrete wavelet packet transform. The application of wavelet packet analysis to the motor stator current is shown to provide a useful diagnostic for incipient bearing fault detection. This continuous monitoring is achieved in a noninvasive manner and without the expense and inconvenience of additional transducers or specialized bearing diagnostic instruments.

The proposed method has several advantages over Fourier analysis tools currently used in motor current signature analysis. Due to the nonstationary nature of the stator current, the wavelet packet transform provides better analysis under varying load conditions. The wavelet packet transform also permits the tailoring of the frequency bands to cover the range of bearing-defect induced frequencies resulting from rotor speed variations. Tailored frequency bands in turn mean a decreased number of inputs and lower complexity for fault detection algorithms such as neural networks. The use of such bands in defect detection is more tolerant of the fact that the actual bearing-defect induced vibration frequencies may vary slightly from the predicted values due to slippage that occurs within the bearing.

References

[1] R. R. Schoen, T. G. Habetler, F. Kamran, and R. G. Bartheld, "Motor bearing damage detection using stator current monitoring," *IEEE Trans. Ind. Applicat.*, vol. 31, pp. 1274–1279, Nov./Dec. 1995.

[2] V. Wowk, *Machinery Vibration, Measurement and Analysis*. New York: McGraw-Hill, 1991.

[3] S. Santoso, E. J. Powers, W. M. Grady, and P. Hoffmann, "Power quality assessment via wavelet transform analysis," *IEEE Trans. Power Delivery*, vol. 11, pp. 924–930, Apr. 1996.

[4] W. Yoon and M. J. Devaney, "Power measurement using the wavelet transform," *IEEE Trans. Instrum. Meas.*, vol. 47, pp. 1205–1210, Oct. 1998.

[5] Y. Zhongming, B. Wu, and A. R. Sadeghian, "Signature analysis of induction motor mechanical faults by wavelet packet decomposition," in *16th Annu. IEEE Applied Power Electronics Conf. Expos.*, vol. 2, 2001, pp. 1022–1029.

[6] M. Vetterli and C. Herley, "Wavelets and filter banks: Theory and design," *IEEE Trans. Signal Processing*, vol. 40, pp. 2207–2232, Sept. 1992.

[7] R. Ansari, "IIR filter banks and wavelets," in *Subband and Wavelet Transforms Design and Applications*. Norwell, MA: Kluwer, 1996.

[8] I. Daubechies, *Ten Lectures on Wavelets*. Philadelphia, PA: SIAM, 1992.

[9] M. V. Wickerhauser, *Adapted Wavelet Analysis From Theory to Software*. Boston, MA: A. K. Limited, 1994.

[10] J. Buckheit and D. L. Donoho, *Software Packet "Wavelab Version 802" of Matlab Program*, 1999.

Levent Eren (M'03) was born in Izmir, Turkey. He recesived the B.S.E.E., M.S., and Ph.D. degrees in electrical engineering from the University of Missouri, Columbia, in 1995, 1998, and 2002, respectively.

He is currently an Assistant Professor at the University of Bahcesehir, Istanbul, Turkey.

Michael J. Devaney (S'60–M'64) was born in St. Louis, MO. He received the B.S.E.E. degree from the University of Missouri, Rolla, in 1964, and the M.S. and Ph.D. degrees in electrical engineering from the University of Missouri, Columbia, in 1967 and 1971, respectively.

He joined the Electrical Engineering Department, University of Missouri, Columbia, in 1969, where he is now a Professor. From 1980 to 1988, he was the Undergraduate Program Director for computer engineering, and, in 1987, he became affiliated with the university's Power Electronics Research Center and served as its Associate Director in 1989 and 1990. He has published 16 journal articles and 41 conference papers. For the past 14 years, has been engaged in research on power metering and power quality measurement supported by Square D.